Optimization for Si Nano-Pillar-Based Broadband Achromatic Metalens

Zhaohui Li and Yihao Lv

***Abstract*—An innovative optimization algorithm, named the hybrid particle swarm and genetic algorithm (PSO_GA), is proposed for designing broadband achromatic metalenses. A database is first constructed by scanning the parameters of the unit cell of the metalenses using FDTD software, mapping each unit cell to its phase modulation capability. The PSO_GA is then utilized to identify the optimal phase matrix that minimizes chromatic aberration for a metalens operating within a specific wave band. Using the PSO_GA, a broadband achromatic metalens is designed and its performance is validated by simulation. The results reveal that the designed metalens successfully focuses light in a wide band (1000 nm∼1250 nm), achieving a mean focusing efficiency of up to 58%. This metalens design method offers a solution for the intelligent design of flat optical devices.**

***Index Terms*—Metalens, near-infrared band, PSO_GA, silicon nanopillar, spot quality.**

I. Introduction

MICRO-NANO photonics has experienced significant growth in the past decade. The advancement in precision manufacturing has led to remarkable progress in utilizing nanostructure materials to manipulate sub-wavelength light fields. In 2011, Capasso et al first proposed the principle of metasurface. Metasurfaces allow for precise manipulation of light fields such as phase, polarization, and amplitude through a thin layer composed of sub-wavelength structural units. Devices based on metasurfaces have proven highly efficient in manipulating optical properties to meet specific applications while avoiding the huge loss caused by light transmission inside the bulk material [1], [2], [3]. Metasurfaces have the advantages of lightweight and easy integration which has important application prospects.

A metalens is an application of metasurface as a focusing lens. It can generate a hyperbolic phase plane producing a focused beam with greater diffraction efficiency [4], [5], [6], [7]. However, due to the wavelength sensitivity of subwavelength structural units, metalens tend to have strong dispersion, which seriously affects their performance in panchromatic optical applications.

Manuscript received 17 January 2024; accepted 22 January 2024. Date of publication 29 January 2024; date of current version 14 February 2024. This work was supported in part by the National Natural Science Foundation of China under Grant 62274124 and in part by the National Natural Science Foundation of China Youth Program under Grant 61705178. *(Corresponding author: Yihao Lv.)*

The authors are with the Xi'an University of Science and Technology, Xi'an 710064, China (e-mail: 1564822216@qq.com; 2607495489@qq.com).

Digital Object Identifier 10.1109/JPHOT.2024.3359324

To solve the chromatic aberration problem of metalens, researchers have proposed a variety of methods. In 2015, Capasso et.al. realized a multi-wavelength achromatic metasurface using dispersion phase compensation [8], manipulating each wavelength to be well-focused at a focal length of 7.5 mm. In 2022, Chen et al. adopted an integrated unit structure composed of silicon pillars and phase plates to realize achromatic metalens with a constant focal length of 32 μm in the wavelength range of 1100∼1500 nm [9]. In the work above, the metalenses are designed by selecting unit structures whose optical response is close to the desired target by calculations and experiences. The initial structure of a metalens is then optimized and fine-tuned by analyzing its performance. This iteration is repeated until the optical response of the metalens meets the design requirements. Unfortunately, there may be deviations in the manual selection of unit structures, and multiple simulations and parameter optimization may time-consuming [10].

Subsequently, Capasso et al introduced a wavelength-only optimization factor into the focusing equation and used a particle swarm optimization algorithm (PSO) to determine the optimization factor value for the full waveband to achieve a reflective achromatic metalens [11]. Recently, Shen et al employed the PSO algorithm to design a phase-modulated-transmissive metalens, realized a broadband achromatic focusing function for a wavelength band of 400 nm to 650 nm, with an identity of its full width at half maximum to its theoretical diffraction limit [12].

Although the PSO algorithm has been utilized in the metalens design, yielding certain outcomes, it remains subject to limitations. Primarily, the design of metalenses is a multiple constraint optimization problem, involving achromatic ability, focusing performance, and transmittance. However, the simplicity inherent in the PSO structure renders it less adept at addressing such intricate optimization problems. Moreover, PSO takes a long time to converge to the optimal solution, leading to a high computing cost in the metalens design.

Furthermore, PSO is sensitive to initial parameters. Different parameter configurations lead to different optimization results. An appropriate parameter initialization requires prior knowledge, which reduces the degree of automation of the design [13], [14], [15].

The Genetic Algorithm (GA), an alternative optimization algorithm, stands out for its distinctive advantages. Firstly, GA operates as a heuristic search algorithm, effectively navigating expansive solution spaces to identify optimal solutions. Secondly, GA exhibits the capacity to dynamically adjust its parameters throughout the search process, enabling the

accommodation of diverse design requirements and constraints. Given that achromatism is typically optimized under wavelength and optical performance constraints, GA emerges as particularly well-suited for metalens design. It excels in navigating complex parameter spaces, facilitating the identification of optimal solutions to minimize chromatic aberration and enhance overall performance metrics.

Moreover, GA employs diverse search strategies, maintaining a population to explore complex solution spaces and mitigating the risk of falling into local optima. This feature enhances its applicability in metalens design, providing it with extensive potential [16]. In summary, the integration of a hybrid algorithm, combining GA and PSO, is anticipated to address the deficiencies of PSO and facilitate a more effective optimization in metalens design.

To achieve the automated design of a broadband achromatic metalens, we initially construct a nanostructure comprising a high-transmittance SiO_2 substrate and high-refractive-index Si cubic pillars. We investigate its modulation characteristics concerning cross-section size variations across a specific wide wavelength range. Subsequently, we present a hybrid algorithm, denoted as PSO_GA, by incorporating GA into PSO, aiming to efficiently explore the optimal phase matrix.

Following the identified optimal phase matrix, we map it onto the size parameters of each unit, realizing a broadband achromatic metalens. The simulations validate that the metalens created using PSO_GA exhibits exceptional achromatic performance. Specifically, it efficiently focuses normal incident plane waves in the band ranging from 1000 nm to 1250 nm onto the desired focal point, with chromatic aberration not exceeding 3 μm along the axis or 1 μm in radius.

II. Broadband Achromatic Metalens Design Principle

To precisely converge a plane wave beam with a wavelength λ, incident perpendicularly through a metalens, to a specified focal point with focal length f, each point on the metalens must impart a specific phase offset φ(R), where R represents the distance from the center of the lens, as shown in (1) [17]:

$$\varphi\ (\mathrm{R}) = -\frac{2\pi}{\lambda}\left(\sqrt{R^2+f^2}-f\right) \tag{1}$$

where $\sqrt{R^2+f^2}$ is the distance of R-points to the focal point (the metalens is located at the z = 0 plane).

Owing to the dispersion effect of the medium on the light wave, a beam with a bandwidth ($\lambda_{\min}$, $\lambda_{\max}$) incident on a lens with a constant focal length f cannot converge onto the same focal point along the optical axis, giving rise to chromatic aberration. Consequently, the phase distribution of the R-points is articulated as a wavelength-dependent function, represented by (2):

$$\varphi_{\mathrm{lens}}\ (R,\lambda) = \varphi\left(R,\lambda_{\max}\right) + \Delta\varphi\left(R,\lambda\right) \tag{2}$$

Where

$$\Delta\varphi\ (\mathrm{R},\lambda) = -\left[2\pi\left(\sqrt{\mathrm{R}^2+f^2}\right)\right]\left(\frac{1}{\lambda}-\frac{1}{\lambda_{\max}}\right)$$

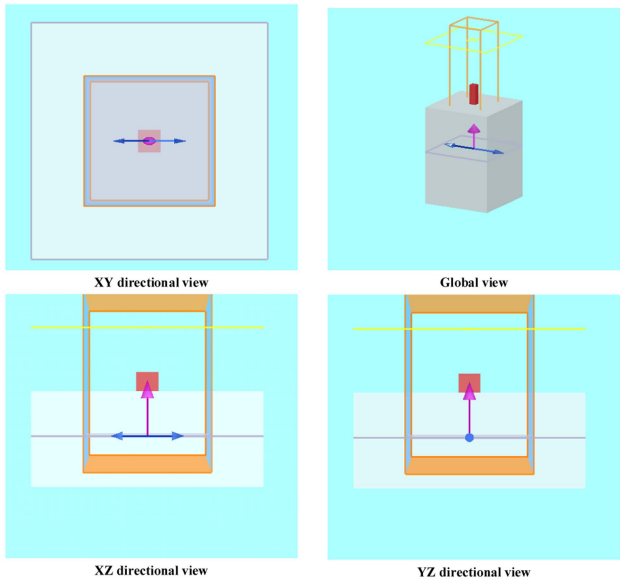

Fig. 1. Nanostructure of Si nanopillar on SiO_2 substrate.

Equation (2) shows that the phase offset is divided into two items. The first item $\varphi(R, \lambda_{\max})$ obtained from (1) is a reference phase, which is only related to $\lambda_{\max}$ and independent of another wavelength. The second item $\Delta\varphi(R, \lambda)$ is proportional to $1/\lambda$ and can be seen as a phase difference between the wave λ and the wave $\lambda_{\max}$.

The objective of achromatic metalens design is to determine optimal structural parameters that yield modulation characteristics closest to $\varphi(R)$ within broad bandwidth constraints. Consequently, the phase distribution $\varphi_{lens}(R, \lambda)$ necessitates correction, ensuring that $\Delta\varphi(R, \lambda)$ remains zero or a constant across all wavelengths, thereby facilitating focal position adjustments.

A constant phase difference $\Delta\varphi(R, \lambda)$ can be achieved by designing the transmission response of each unit structure of metalens. Due to the sensitivity of nanostructure to wavelengths, an optimization factor C(λ) is introduced to fix $\Delta\varphi(R, \lambda)$ by a phase compensation for specific wavelengths. Therefore, the phase distribution of achromatic metalens is rewritten as (3):

$$\varphi_{lens}\ (R,\lambda) = \varphi\left(R,\lambda_{max}\right) + \Delta\varphi\left(R,\lambda\right) + C\left(\lambda\right) \tag{3}$$

The ideal phase, $\varphi_{lens}(R)$, is directly computed from the desired achromatic metalens, whereas the actual phase arises from the modulation of unit structures by the incident wave. It is imperative to examine the modulation characteristics of nanostructures, establishing a comprehensive database delineating the response function of structural parameters to wavelengths. Subsequently, the selection of each unit structure is contingent upon meeting the specified modulation criteria.

III. Establishment of a Database on the Response of Nano-Structures

A unit cell of a nanostructure is shown in Fig. 1, which is consisted of a Si pillar built on a SiO_2 substrate. The local phase modulation function of the metalens is determined by the units,

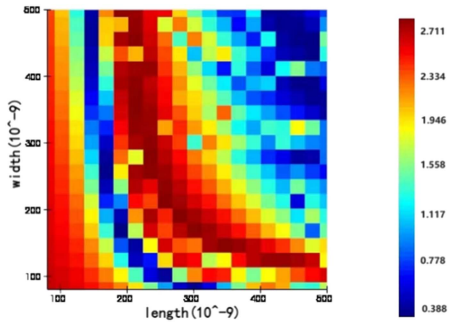

Fig. 2. Modulation characteristics of nanostructure at wavelength of 1000 nm.

including their material and structural parameters. When the material is fixed, the shape of the Si pillar is varying and its modulation characteristics are investigated. The shape of the nanostructure in this study is chosen as a pillar with a rectangular cross-section, due to its excellent optical properties, simplicity, and compact size for easy modularity.

The initial parameters of the nanostructure need to be set. A unit of metalens for focusing should satisfy a phase modulation range of 0∼2π. It has been verified that the phase modulation range of the Si pillar with a fixed-cross-section is expended with its height increasing [2]. By fixing the height while varying the length and width of the cross-section of the Si pillar, its phase modulation function is achieved.

The nanostructure is built in a numerical simulation software FDTD, within the simulation area and virtual monitors configurations shown in Fig. 1. The height of it is set to 0.6 μm constantly, due to the fabrication limitation. Since the minimum manufacturing size at current is limited to 0.08 μm, and the maximum size is the center-to-center distance of two adjacent units, the length l and the width w of the nano-pillar's cross-section are both set in the range of (0.08 μm, 0.5 μm).

By scanning the parameters l and w, the nanostructure's modulation properties for different wavelengths are obtained from FDTD simulation. The scanning range for l and w both from $\mathrm{d_{min}} = 0.08$ μm to $\mathrm{d_{max}} = 0.5$ μm, with a scanning step $\Delta \mathrm{d} = 0.021$ μm. Six wavelengths ($\lambda_0 = 1000$ nm, $\lambda_1 = 1050$ nm, $\lambda_2 = 1100$ nm, $\lambda_3 = 1150$ nm, $\lambda_4 = 1200$ nm, $\lambda_5 = 1250$ nm) are selected as representations of the operating band ($\lambda_{\min}$, $\lambda_{\max}$) = (1000 nm, 1250 nm) to investigate the modulation characteristics of nanostructures. The modulation characteristics database $\varphi[l,w,\lambda]$ is constructed, and one slice at $\lambda_0 = 1000$ nm is painted as a false-color image in Fig. 2. It can be seen that the phase modulation range covers [-π,π], and so does at other representation wavelength.

IV Hybrid Algorithm of Particle Swarm and Genetic Algorithm to Find Optimal Solution

The objective in metalens design is to minimize the distance between the ideal phase modulation, as computed from the desired configuration, and the actual phase modulation imparted by the unit structure at each wavelength. This objective is equivalent to minimizing an error function, denoted as ε in (4).

$$\varepsilon = \sum_{\lambda=\lambda_0}^{\lambda_5} \sum_{\mathrm{R}=0}^{\mathrm{R_{max}}} \left|\varphi\left(\mathrm{R}\right) - \varphi_{\mathrm{lens}}\left(\mathrm{R},\lambda\right)\right| \tag{4}$$

Hence, the problem of metalens design transforms into a problem of solving $C(\lambda)$ to ensure that (4) converges to its minimum. The particle swarm optimization algorithm coupled with the genetic algorithm (PSO_GA) offers a viable approach to seek the optimal $C(\lambda)$.

The PSO_GA is a hybrid approach wherein the GA is integrated into the framework of the PSO. Within the PSO_GA framework, the population undergoes updates through the crossover and mutation operations of GA, converging towards the optimal solution that corresponds to the minimum fitness value during the iteration of the PSO loop. The crossover operator plays a crucial role in enhancing global search capabilities, mitigating the risk of local optima. Consequently, it is anticipated that the optimization performance of PSO_GA will be significantly improved [18], [19].

A broadband achromatic metalens with numerical aperture N.A. = 0.5 and focal length $f = 6.5\mu$m is designed. The specific procedure to obtain the optimal $C(\lambda)$ using PSO_GA is as follows:

Step 1: Initializing population. First, random values between (0,2π) are taken as the initial population C^0 of $C(\lambda)$. For our metalens, a vector ${C_j}^0$ is assigned to each representative wavelength, which denoted by a subscript j. 30 random real numbers are assigned to a vector ${C_j}^0$ with its location being denoted by another subscript i. Thus, $C^0(\lambda)$ is discretized into a vector space ${C_{i,j}}^0$ with dimension of 30 × 6, or the population ${C_{i,j}}^0$. Second, another random matrix with 30 × 6 valued between (01) is taken as the initial vector ${v_{i,j}}^0$ of population velocity v^0. Third, all the fitness ${\varepsilon_i}^\circ$ for each particle ${C_i}^0$ in the population C^0 are computed according to (4), composing an initial population fitness ε^0. Finally, the optimal particle C_a is found by seeking the minimum of ε^0 of population C^0, i.e., ${\varepsilon_a}^0 = \min\{\varepsilon^0\}$.

Step 2: Updating population ${C_{i,j}}^0$ by PSO. The *jth* column vector ${C_j}^t$at the *(t+1)th* iteration is calculated into *C'* as (5). The parameters are set as follows: the inertia factor $m = 0.8$, the individual learning factor $c_1 = 1.49445$, and the population learning factor $c_2 = 1.49445$, ${r_1}^t$ and ${r_2}^t$ are random numbers within [01], which are refreshed at each iteration.

$$\begin{aligned} v_{ij}^{t+1} &= m v_{ij}^t + c_1 r_1^t \left[\varepsilon^t - C_{ij}^t\right] + c_2 r_2^t \left[\varepsilon_a^t - C_{ij}^t\right] \\ C'_{ij} &= C_{ij}^t + v_{ij}^{t+1} \end{aligned} \tag{5}$$

Step 3: Crossover and mutation by GA.

First, crossover operation: The *i1*th and *i2*th particles, or two row vectors ${C_{i1}}'$ and ${C_{i2}}'$, which are randomly selected from *C'*, are crossovered by (6), transformed into ${C_{i1}}''$ and ${C_{i2}}''$; And then, ${C_{i1}}'$ and ${C_{i2}}'$ are replaced by ${C_{i1}}''$ and ${C_{i2}}''$ respectively to obtain population *C''*; Parameters β_1, β_2 in (6) are random numbers with the values of (01).

$$C''_{i1} = \beta_1^T \cdot C'_{i1} + (1-\beta_1)^T \cdot C'_{i2}$$

TABLE I
VALUES OF OPTIMAL FACTOR C(λ)

Wavelength /nm	C(λ)
1000	0.4103
1050	2.7637
1100	3.3277
1150	4.1021
1200	5.6743
1250	6.1281

$$C''_{i2} = \beta_2^T \cdot C'_{i1} + (1-\beta_2)^T \cdot C'_{i2} \tag{6}$$

Second, variation operation: A random vector T_{ij} valued from (01) with dimension of 10×6 is generated, and then is amplified and offset to transform into T_{ij}", and substitutes 10 rows vectors C_{pj} selected randomly from population C". At which point, population C^0 is updated into population C^1, as described as (7):

$$\begin{aligned} T''_{ij} &= 2\pi \cdot T_{ij} + 2\pi \\ C''_{pj} &= T''_{ij} \end{aligned} \tag{7}$$

where the subscript p denotes a random selection.

Step 4: Updating population fitness. The ${\varepsilon_i}^1$ of particle ${C_i}^1$ are calculated with (4) to compose fitness ε^1 of population C^1. The optimal particle ${C^1}_a$ is found by seeking the minimum of ε^1 of population C^1, which is same as the operation in Step1. At which point, an iteration cycle is complete, to continue the iteration again with Step 2.

Step 5: Optimization break. The iteration goes on until the fitness ε^N is below a pre-set threshold. The optimal particles ${C_a}^N$ corresponding to the minimum fitness ${\varepsilon_a}^N$ is returned as the final result.

The best $C(\lambda)$ values for 6 wavelengths obtained by using PSO_GA are listed in Table I.

The convergence and stability of PSO_GA are verified with a comparison among PSO, GA, and PSO_GA, which is demonstrated in Fig. 3.

Fig. 3(a) illustrates the values of fitness value ε_a of the three algorithms during iterations, noted by different line types. It can be seen that the PSO_GA's curve (solid line with triangles) directly and rapidly drops to a minimum after a few iteration cycles, being steeper and smoother than the curves of PSO (dash line with dots) and GA(dash line with triangles), which indicates an excellent convergence of PSO_GA. Fig. 3(b) presents the results of running the Monte Carlo experiment 10 times on the three algorithms respectively. The correlations of the optimal solution at each time to the one at the first time are calculated and plotted. It can be observed that the correlation curve of PSO_GA fluctuates little over multiple runs, while the curves of PSO and GA have large fluctuations, indicating that PSO_GA exhibits better stability.

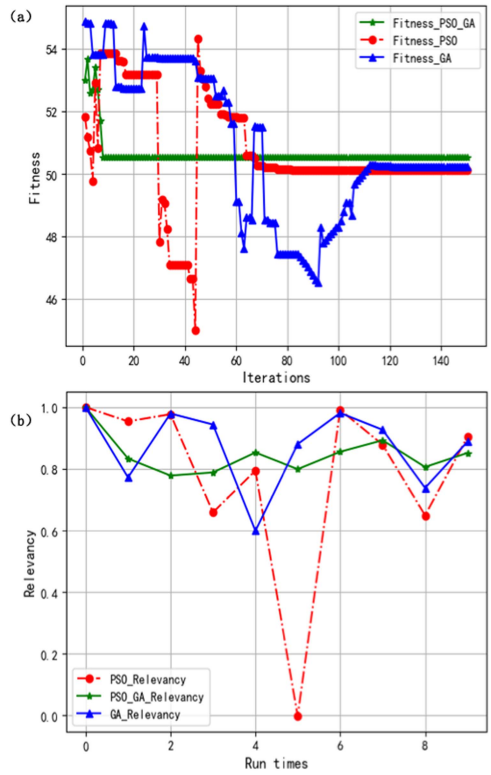

Fig. 3. Performance comparison among PSO, GA, and PSO_GA. (a) convergence curves; (b) correlations of the optimal solution to the initial one at Monte Carlo experiment with 10 times.

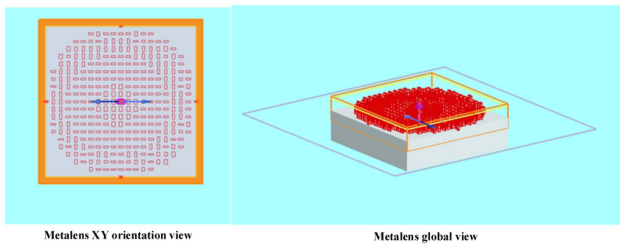

Fig. 4. Metalens composed of Si-nanopillar-SiO_2-substrate nanostructures.

V. EXPERIMENTAL VALIDATION

A. *Metalens Construction on the Optimal* C(λ)

The optimal $C(\lambda)$ values for each wavelength are brought into (3) to produce the optimal phase of the metalens. Note that the diameter of metalens is discretized with an interval of 0.5μm as well. $\varphi_{lens}(R, \lambda)$ at the radial distance R is mapped to the cross-section size of the unit nanostructure by the nearest table lookup method from the database $\varphi[l,w,\lambda]$. Since the mapping of $\varphi_{lens}(R, \lambda)$ to $\varphi[l,w,\lambda]$ is a discrete quantization process, the maximum quantization error is half of the scanning step, $\Delta d/2 = 0.0105\mu$m. The size parameters of the unit nanostructure at every discrete radial distance are obtained. The whole metalens can be constructed through a rotationally symmetric extension performed on the units distributed along the diameter. A circular metalens with a diameter of 5.2μm is constructed as shown in Fig. 4, in which 20 micro-unit structures on diameter.

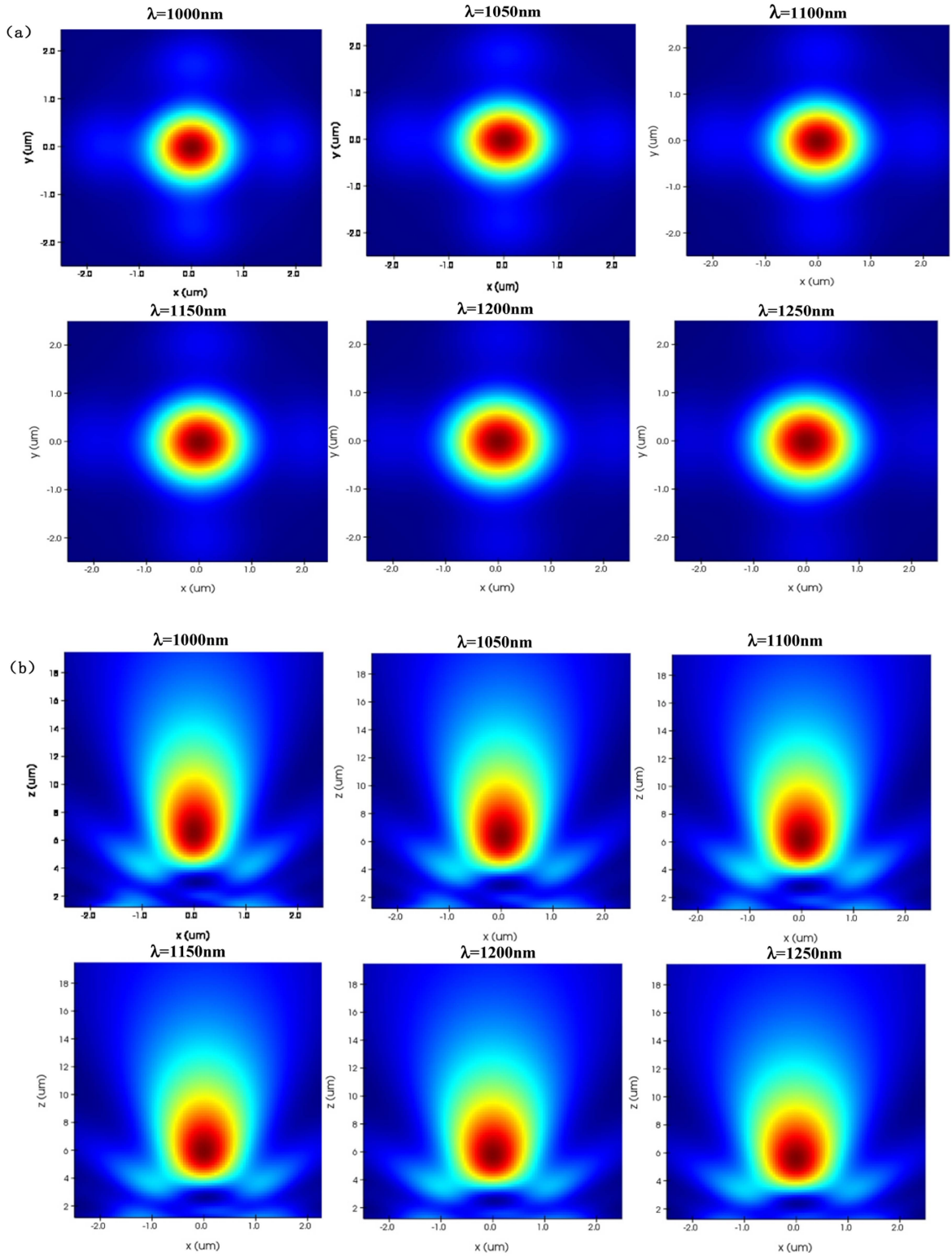

Fig. 5. Focused light intensity of metalens for 6 wavelengths. (a) Transverse intensity diagram at focal plane; (b) axial intensity diagram near focal point.

B. Achromatic Performance Verification

After getting the metalens mode, its achromatic performance should be measured. In the numerical simulation software FDTD, 6 plane waves with the representative wavelengths above illuminating the metalens, the intensity distribution near focal point is calculated and drawn in false color images in Fig. 5. Fig. 5(a) is the transverse intensity of the focused light field at the focal plane (at the distance of $z = 6.5\mu$m for the metalens), where the Airy disks for different wavelengths are relatively similar.

TABLE II
COMPARISON OF FOCAL SPOT QUALITY OF METALENS OPTIMIZED THOUGH PSO, GA, AND PSO_GA

Wavelength /nm	Diffraction limit /m	FWHM(PSO) /m	FWHM(PSO_GA) /m	FWHM(GA) /m
1000	0.86e-6	1.096e-6	0.896e-6	0.956e-6
1050	0.903e-6	1.136e-6	1.024e-6	1.115e-6
1100	0.946e-6	1.152e-6	1.024e-6	1.256e-6
1150	0.989e-6	1.372e-6	1.224e-6	1.354e-6
1200	1.032e-6	1.476e-6	1.327e-6	1.422e-6
1250	1.075e-6	1.656e-6	1.316e-6	1.483e-6
Diffraction limit and minimum error of FWHM		0.581e-6	0.413e-6	0.259e-6

Fig. 5(b) is the axial intensity distribution near the focal point, where the focal lengths corresponding to different wavelength are all around 6.5μm.

To quantitatively evaluate the focusing performance of the broadband achromatic metalens, its focal spot quality and focusing efficiency are calculated. In addition, the metalenses constructed by PSO, GA, and PSO_GA respectively are evaluated to demonstrate the superiority of POS_GA.

Focal spot quality is measured by the distance of Airy disk diameter, or the Full Width at Half Maximum (FWHM), to the theoretical diffraction limit of the lens. The closer the FWHM is to the diffraction limit, the better the spot quality. By measuring the diffraction limits, the FWHMs, and the differences between them for the represented wavelengths, the maximum distance of FWHM to diffraction limit resulted from PSO, GA and PSO_GA is $err_{max1} = 0.581\mu$m, $err_{max2} = 0.413\mu$m, and $err_{max3} = 0.259\mu$m, respectively, listed in Table II. In this comparison, the minimum difference of FWHM to diffraction limit is acquired under PSO_GA's column, indicating a good focal spot quality when using PSO_GA optimizing metalens.

Focusing efficiency is measured by the ratio of the intensity of the light reaching the focus to the total energy of the incident beam. By calculating the intensity within the Airy disk, the focusing efficiencies at different represented wavelengths of the metalens constructed by PSO, GA, and PSO_GA are obtained respectively, as plotted in Fig. 6. It can be seen that the focusing efficiency curve of PSO_GA floats much higher than that of PSO and GA, with the average value being 58% and peak value up to 60%. While the average focusing efficiency values of PSO and GA are around 29%. In this comparison, the high and flat curve of PSO_GA, indicating an outstanding and balanced focusing efficiency when using PSO_GA optimizing metalens.

To sum up, the broadband achromatic metalens constructed by PSO_GA has excellent performances, within a rapid, stable convergent optimization process.

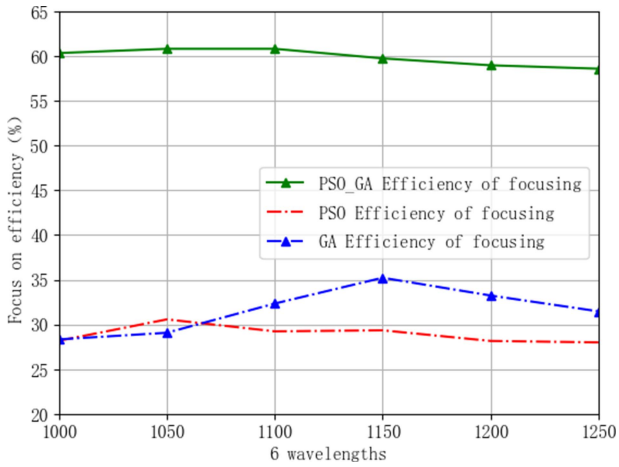

Fig. 6. Comparison of focusing efficiency of metalens optimized though PSO, GA, and PSO_GA.

VI SUMMARY

In this paper, we present the construction of an achromatic metalens comprising nanostructures of Si pillars on a SiO_2 substrate, designed to operate in the infrared band ranging from 1000 nm to 1250 nm. The detailed design and optimization process are outlined, encompassing the principles of chromatic correction, the establishment of a modulation characteristic database for the nanostructure, and the optimization using the PSO_GA algorithm to determine chromatic correction factors. The metalens is constructed after determining the size parameters of each cell unit based on the optimal phase. FDTD simulations confirm the excellent focusing performance of the metalens. Furthermore, the superiority of the hybrid algorithm PSO_GA is validated. In comparison to the original PSO and GA, PSO_GA exhibits enhanced stability and rapid convergence. Its optimization results markedly improve the quality of focal spots and the efficiency of focusing.

REFERENCES

[1] N. Yu et al., "Light propagation with phase discontinuities: Generalized laws of reflection and refraction," *Science*, vol. 334, no. 6054, pp. 333–337, 2011.
[2] Y. Xiaobo et al., "Photonic spin hall effect at metasurfaces," *Science*, vol. 339, pp. 1405–1407, 2013.
[3] N. Xingjie et al., "An ultrathin invisibility skin cloak for visible light," *Science*, vol. 349, no. 6254, pp. 1310–1314, 2015.
[4] K. Dou et al., "Off-axis multi-wavelength dispersion controlling metalens for multi-color imaging," *Opto-Electron. Adv.*, vol. 3, no. 4, 2020, Art. no. 190005.
[5] S. Shrestha et al., "Broadband achromatic dielectric metalenses," *Light: Sci. Appl.*, vol. 7, no. 1, 2018, Art. no. 85.

[6] Y. Li et al., "Achromatic flat optical components via compensation between structure and material dispersions," *Sci. Rep.*, vol. 6, no. 1, 2016, Art. no. 19885.
[7] C. Yan et al., "Midinfrared real-time polarization imaging with all-dielectric metasurfaces," *Appl. Phys. Lett.*, vol. 114, no. 16, 2019, Art. no. 161904.
[8] Z. Zhao et al., "Multispectral optical metasurfaces enabled by achromatic phase transition," *Sci. Rep.*, vol. 5, no. 13, 2015, Art. no. 15781.
[9] C. Yufeng, H. Lingling, L. Bingyi, A. Kang, L. Zengliang, and W. Yongtian, "Broadband achromatic metalens and meta-deflector based on integrated metasurface," *J. Phys. D: Appl. Phys.*, vol. 55, no. 2, 2022, Art. no. 15248.
[10] A. Xi-Peng, *Broadband Achromatic Metalenses Design based On Deep Learning*. Wuhan, China: Huazhong Univ. Sci. Technol., 2021.
[11] M. Khorasanineja et al., "Achromatic metalens over 60 nm bandwidth in the visible and metalens with reverse chromatic dispersion," *Nano Lett.*, vol. 17, no. 3, pp. 1819–1824, 2017.
[12] S. Yi-Jia et al., "Achromatic metalens based on coordinative modulation of propagation phase and geometric phase ," *Opto-Electron. Eng.*, vol. 47, no. 10, pp. 110–118, 2020.
[13] F. Ricardo, N. C. Gonçalo, and C. A. Carlos, "An elitist multi-objective particle swarm optimization algorithm for composite structures design," *Composite Struct.*, vol. 31, 2022, Art. no. 300.
[14] X. Liu, Z. Li, P. Xu, and J. Li, "Joint optimization for bandwidth utilization and delay based on particle swarm optimization," *IEEE Access*, vol. 9, pp. 92125–92133, 2021.
[15] A. U. Rehman, A. Islam, and S. B. Belhaouari, "Belhaouari samir brahim. multi-cluster jumping particle swarm optimization for fast convergence," *IEEE Access*, vol. 8, pp. 189382–189394, 2020.
[16] L. Tian-Wei, B. Jiang-Bo, F. Nicholas, B. Guang-Yu, and L. Dong, "Multi-objective optimisation designs for thin-walled deployable composite hinges using surrogate models and genetic algorithms," *Composite Struct.*, vol. 280, 2022, Art. no. 25360.
[17] M. García-Carrillo, A. B. Espinoza-Martínez, L. F. Ramos-de Valle, and S. Sánchez-Valdés, "Simultaneous optimization of thermal and electrical conductivity of high density polyethylene-carbon particle composites by artificial neural networks and multi-objective genetic algorithm," *Comput. Mater. Sci.*, vol. 201, 2022, Art. no. 110956.
[18] S. Kanwal et al., "High-efficiency, broadband, near diffraction-limited, dielectric metalens in ultraviolet spectrum," *Nanomaterials*, vol. 10, no. 3, 2020, Art. no. 26845.
[19] H. Garg, "A hybrid PSO-GA algorithm for constrained optimization problems," *Appl. Math. Computation*, vol. 274, pp. 292–305, 2016.